ACS OMEGA

Open Access



http://pubs.acs.org/journal/acsodf

Article

# A PD-L1-Targeted Probe Cy5.5-A11 for *In Vivo* Imaging of Multiple Tumors

Xiao-Cheng Cao,[#] Xue-Li Mao,[#] Shan-Shan Lu, Wei Zhu, Wei Huang, Hong Yi, Li Yuan, Jian-Hua Zhou, and Zhi-Qiang Xiao*

Cite This: *ACS Omega* 2024, 9, 43826−43833

Read Online

ACCESS | Metrics & More | Article Recommendations

**ABSTRACT:** PD-L1 is an immune checkpoint molecule mediating cancer immune escape, and its expression level in the tumor has been used as a biomarker to predict response to immune checkpoint inhibitor (ICI) therapy. Our previous study reveals that an 11 amino acid-long ANXA1-derived peptide (named A11) binds and degrades the PD-L1 protein in multiple cancers and is a potential peptide for cancer diagnosis and treatment. Near-infrared fluorescence (NIF) optical imaging of tumors offers a noninvasive method for detecting cancer and monitoring therapeutic responses. In this study, an NIF dye Cy5.5 was conjugated with A11 peptide to develop a novel PD-L1-targeted probe for molecular imaging of tumors and monitor the dynamic changes in PD-L1 expression in tumors. *In vitro* imaging studies showed that intense fluorescence was observed in triple-negative breast cancer MDA-MB-231, nonsmall cell lung cancer H460, and melanoma A375 cells incubated with Cy5.5-A11, and the cellular uptake of Cy5.5-A11 was efficiently inhibited by coincubation with unlabeled A11 or knockdown of cellular PD-L1 by shRNA. *In vivo* imaging studies showed accumulation of Cy5.5-A11 in the MDA-MB-231, H460, and A375 xenografts with good contrast from 0.5 to 24 h after intravenous injection, indicating that Cy5.5-A11 possesses the strong ability for *in vivo* tumor imaging. Moreover, the fluorescent signal of A11-Cy5.5 in the xenografts was successfully blocked by coinjection of unlabeled A11 peptide or knockdown of cellular PD-L1 by shRNA, indicating the specificity of Cy5.5-A11 targeting PD-L1 in tumor imaging. Our data demonstrate that Cy5.5-A11 is a novel tool for tumor imaging of PD-L1, which has the potential for detecting cancer and predicting ICI therapeutic responses.

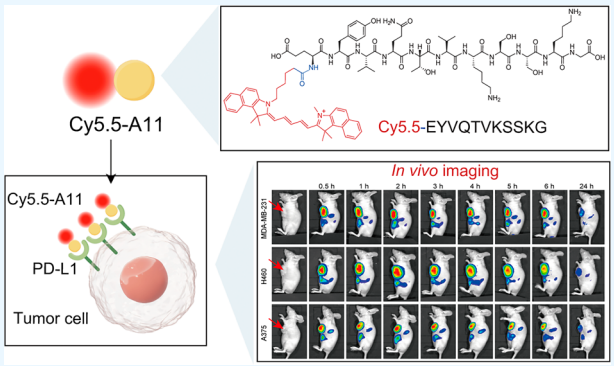


## INTRODUCTION

Anti-PD-1/PD-L1 antibody-based immune checkpoint inhibitor (ICI) therapy represents a substantial therapeutic breakthrough in cancer therapy and shows notable therapeutic advantages in the treatment of multiple advanced cancers.[1,2] Nonetheless, less than 30% of cases across various cancer types respond to ICI therapy, and a substantial number of individuals do not benefit from this treatment.[2] Therefore, developing a tool for predicting response to ICI therapy will provide valuable information for personalized immunotherapy.

Interaction of PD-1 and PD-L1 stimulates substantial changes within the tumor microenvironment and disturbs the function of effector T cells, resulting in tumor immune evasion.[3,4] Multiple inhibitory ligands expressed on the surface of cancer cells represent a significant feature of tumor immune escape, notably PD-L1.[5] PD-L1 functions as an inhibitory mechanism that dampens antitumor immunity by interacting with the PD-1 receptor. Furthermore, anti-PD-1/PD-L1 antibody treatment is preferred by patients whose cancer cells express PD-L1.[6] Therefore, PD-L1 is acknowledged as a vital target in cancer immunotherapy.

PD-L1 expression serves as a critical biomarker that enables the identification of cancer patients anticipated to receive favorable responses from ICI treatment, facilitating the selection of appropriate candidates for therapy.[7] PD-L1 expression levels are evaluated clinically through immunohistochemistry (IHC) on tumor samples acquired via invasive methods, which involve surgical procedures and biopsies.[8,9] PD-L1 expression in tumors has been suggested to be dynamic[10,11] and regulated by treatment including radiotherapy.[12,13] However, dynamic variations in PD-L1 expression cannot be detected by IHC. Furthermore, PD-L1 levels

Received: July 22, 2024
Revised: October 1, 2024
Accepted: October 7, 2024
Published: October 17, 2024

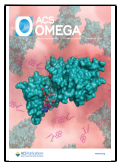

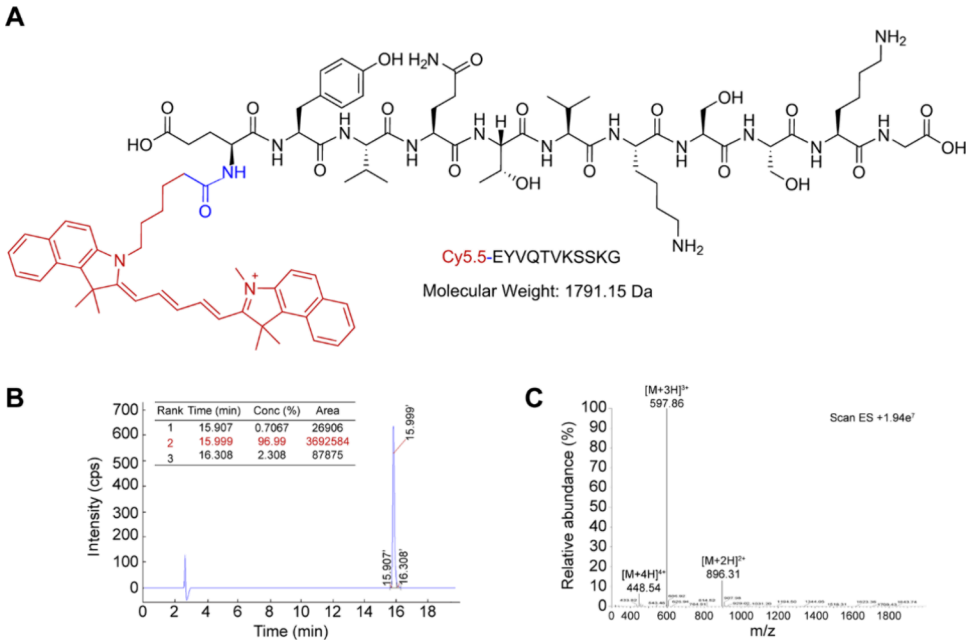


**Figure 1.** Chemical structure and characterization of Cy5.5-A11. (A) Chemical structure of Cy5.5-A11. The red section represents the near-infrared fluorescent Cy5.5 dye, the blue section represents an amido bond, and the black section represents A11 (EYVQTVKSSKG). (B) Chromatogram of Cy5.5-A11 in the time range of 0−20 min. The retention times, concentrations , and areas of three chromatographic peaks are shown in the inserted table. The retention time, concentration, and area of Cy5.5-A11 are highlighted in red. (C) Identification of Cy5.5-A11 by MS. The total molecular weights of three parent ions [896.31, $(M + 2H)^{2+}$; 597.86, $(M + 3H)^{3+}$; and 448.54, $(M + 4H)^{4+}$] are 1791.15 Da, which is consistent with the molecular weight of Cy5.5-A11.

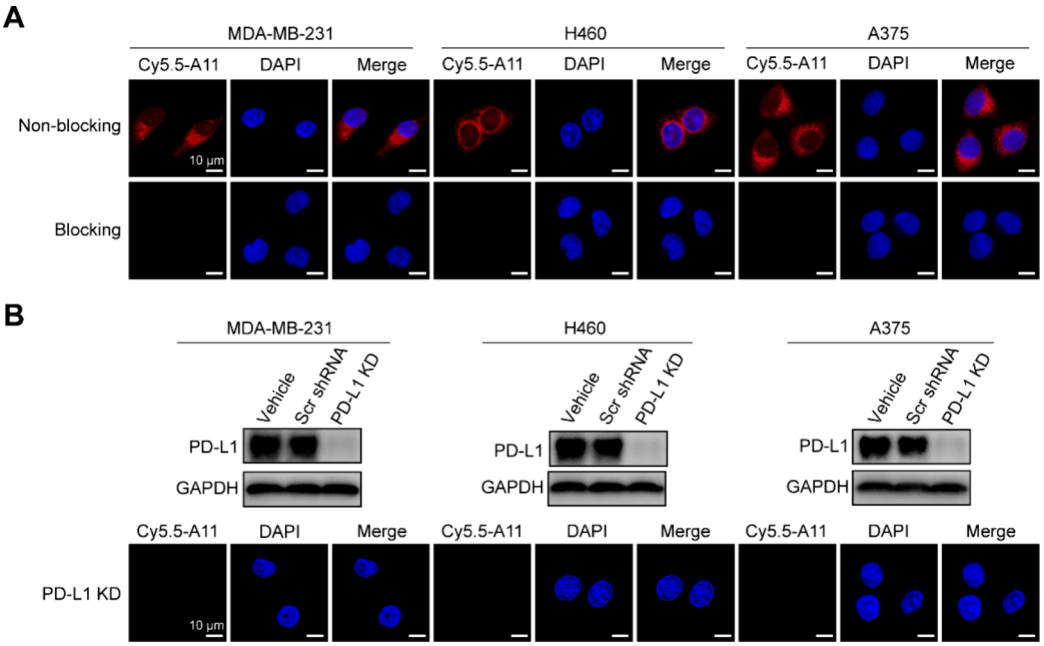


**Figure 2.** Cy5.5-A11 as a PD-L1-targeted probe for *in vitro* imaging of cancer cells. (A) Confocal microscopy images of MDA-MB-231, H460, and A375 cells incubated with 10 nM Cy5.5-A11 probe (nonblocking) or 10 nM Cy5.5-A11 probe in the presence of 1 $\mu$M unlabeled A11 (blocking). (B) Fluorescent signal is not observed in the PD-L1 knockdown MDA-MB-231, H460, and A375 cells incubated with 10 nM Cy5.5-A11 probe. (*top*) Western blot showing the levels of PD-L1 in MDA-MB-231, H460, and A375 cells with PD-L1 knockdown and their corresponding control cells. (*bottom*) Confocal microscopy images of PD-L1 knockdown cancer cells incubated with 10 nM Cy5.5-A11 probe. The scale was 10 $\mu$m. KD, knockdown. Scr shRNA, scrambled shRNA.

assessed by IHC are sometimes reliant on a solitary sample or several tiny biopsies, which may not accurately reflect the actual state of PD-L1 expression owing to the heterogeneity of the tumor.[14−16] Moreover, tumor biopsy is not always feasible when the lesion location is inaccessible. These limitations underscore the necessity for methods to evaluate whole-body PD-L1 expression levels for better recognition of cancer patients eligible for ICI therapy. Unlike IHC, molecular imaging of PD-L1 through noninvasive techniques facilitates quantitative and real-time evaluation of dynamic whole-body


https://doi.org/10.1021/acsomega.4c06761
ACS Omega 2024, 9, 43826−43833

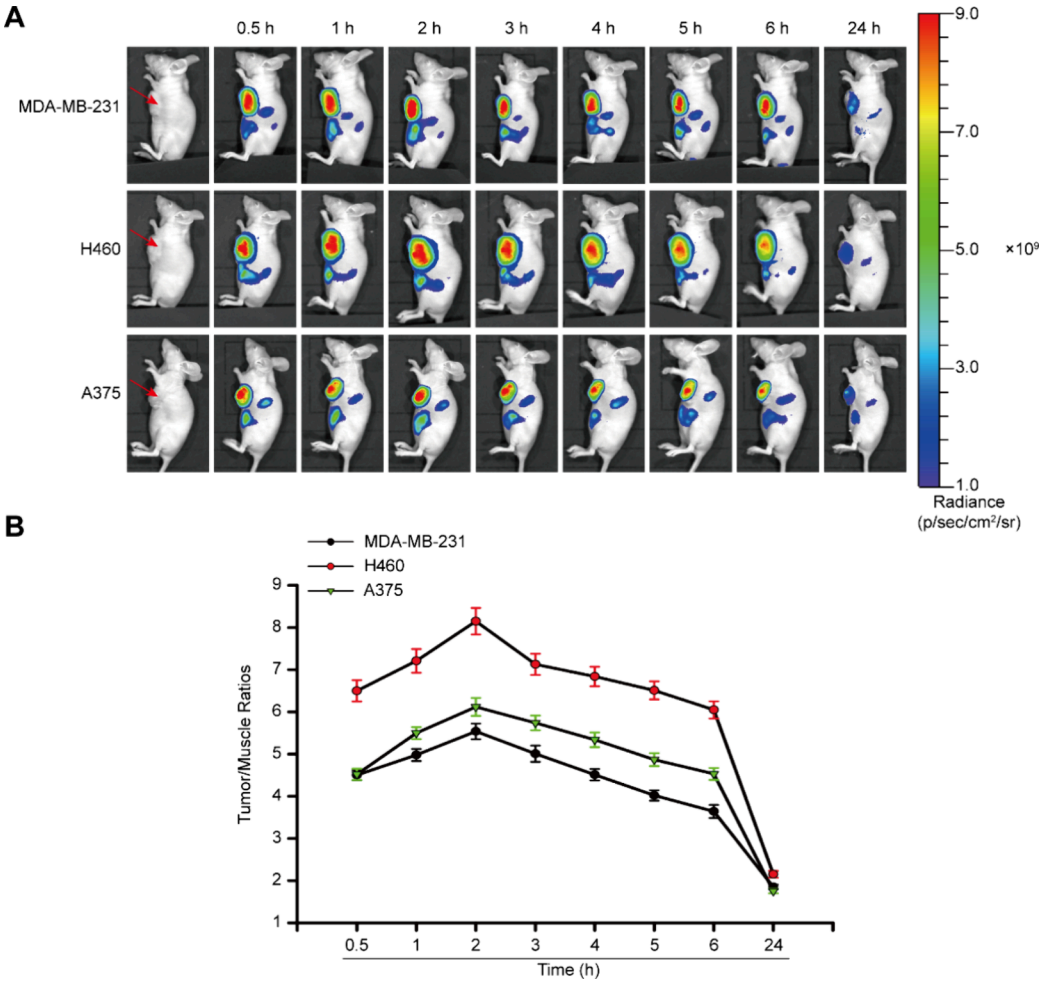


**Figure 3.** *In vivo* NIR fluorescence imaging studies of MDA-MB-231, H460, and A375 tumor-bearing mice using the Cy5.5-A11 probe. (A) Photograph and NIR fluorescent images of mice intravenously injected with the Cy5.5-A11 probe. The images were acquired at 0.5, 1, 2, 3, 4, 5, 6, and 24 h p.i. The red arrows indicate the tumors. (B) Region-of-interest (ROI) study of the tumor/muscle tissue ratio of the Cy5.5-A11 probe in the imaging mice ($n$ = 3). To determine tumor contrast, mean fluorescence intensities of the tumor area at the right shoulder of the animal and the muscle tissue at the surrounding tissue were calculated using the ROI function of IVIS Living Image 4.3.1 software.

PD-L1 levels,[17−20] which would be beneficial to guide ICI therapy.

Our previous study found that an 11 amino acid-long ANXA1-derived peptide (EYVQTVKSSKG), A11 peptide, binds and degrades PD-L1 in various cancer cells[21] and exhibits antitumor immunity via degrading the PD-L1 protein.[21] Since A11 not only binds to PD-L1 but also inhibits immune escape in multiple cancers, it is a perfect vehicle for *in vivo* PD-L1 imaging of tumors and targeted tumor therapeutics.

The development of noninvasive optical imaging technologies is very desired for the purpose of cancer diagnosis and monitoring therapeutic response.[22,23] The majority of the wavelength employed in near-infrared fluorescence (NIF) imaging is between 700 and 900 nm, at which the absorbance and autofluorescence of biomolecules are minimal. Therefore, NIF optical imaging is a promising technology for *in vivo* visualization of tumors at the molecular level.[24,25] This imaging method is cost-effective, highly sensitive, and devoid of ionizing radiation, making it a powerful tool for early-stage cancer detection, therapy response evaluation, and drug development.[26] This study develops an NIF optical probe, Cy5.5-A11, derived from the binding of A11 to the PD-L1 protein.[21] This probe was developed for *in vitro* and *in vivo* PD-L1 molecular imaging, offering significant information about PD-L1 expression in malignancies in the whole body.

## RESULTS

**Characterization of Cy5.5-A11.** Our previous study found that A11 peptide binds to PD-L1 in multiple tumors.[21] Therefore, the C-terminal of the NIF Cy5.5 dye was conjugated with the N-terminal of A11 peptide through the amido bond to construct a PD-L1-targeted probe Cy5.5-A11 (ChinaPeptides). The molecular structure of Cy5.5-A11 is displayed in Figure 1A. The crude product of synthesized Cy5.5-A11 was purified by HPLC, and a chromatographic peak component was obtained in 15.999 min, with a peak purity of 96.99% (Figure 1B). Subsequently, this chromatographic peak component was analyzed by ESI-MS, and three parent ions, 896.31, $(M + 2H)^{2+}$; 597.86, $(M + 3H)^{3+}$; and 448.54, $(M + 4H)^{4+}$, were identified (Figure 1C). The total molecular weights of the 3 parent ions are 1791.15 Da, which is consistent with the molecular weight of Cy5.5-A11.

***In Vitro* Fluorescence Imaging of Cy5.5-A11.** To explore whether Cy5.5-A11 serves as a PD-L1-targeted probe for imaging of live cancer cells, MDA-MB-231, H460, and


https://doi.org/10.1021/acsomega.4c06761
ACS Omega 2024, 9, 43826−43833

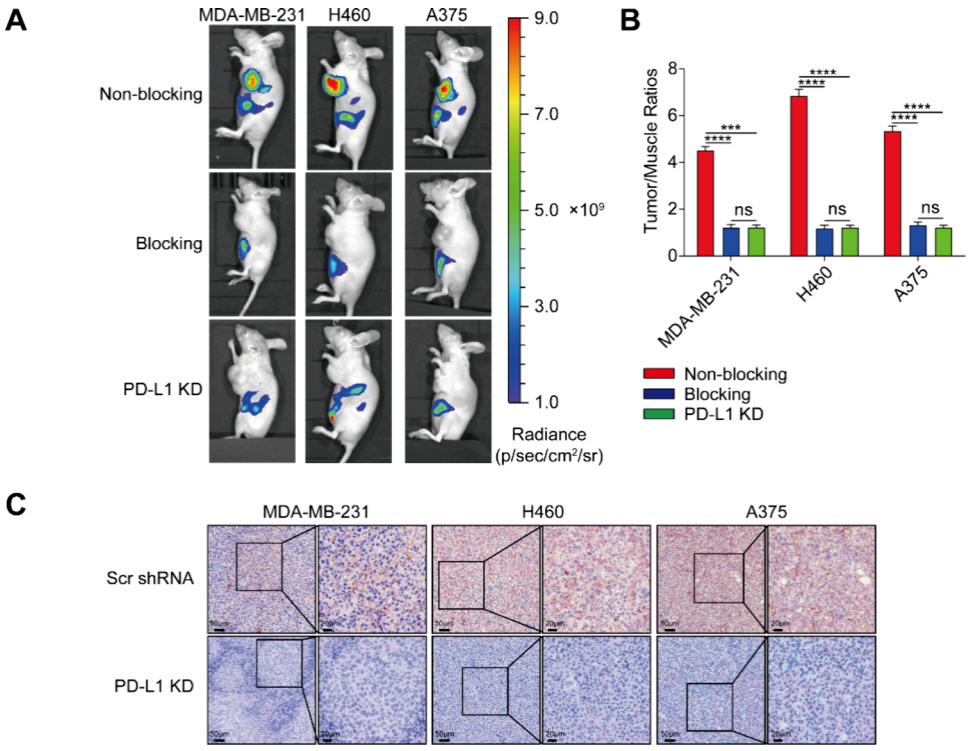


**Figure 4.** Tumor target specificity of the Cy5.5-A11 probe for *in vitro* tumor imaging. (A) Representative optical fluorescence imaging of MDA-MB-231, H460, and A375 tumor-bearing mice in the nonblocking (*top*) and blocking groups (*middle*), as well as PD-L1 knockdown MDA-MB-231, H460, and A375 tumor-bearing mice (*bottom*). Tumor-bearing mice were intravenously injected with 1 nM Cy5.5-A11 or a mixture of 1 nM Cy5.5-A11 and 1 $\mu$M unlabeled A11 and subjected to whole-body imaging 4 h p.i. (B) Fluorescence intensity ratio of tumor-to-muscle based on the ROI analysis at 4 h p.i. in the three groups of mice. (C) Representative IHC showing PD-L1 expression levels in the xenografts of PD-L1 knockdown cancer cells and scrambled shRNA control cancer cells. Data represent mean ± SD. Statistical differences were determined by Student's *t* test. ***, $P < 0.001$; ****, $P < 0.0001$.

A375, originating from triple-negative breast cancer, nonsmall cell lung cancer (NSCLC), and melanoma, respectively, were incubated with 10 nM Cy5.5-A11 probe or a mixture of 10 nM Cy5.5-A11 probe and 1 $\mu$M unlabeled A11 at 37 °C for 6 h and observed using laser confocal microscopy. As shown in Figure 2A, the three types of cancer cells exhibited a robust fluorescent signal, which was successfully blocked when incubated with excess unlabeled A11 (1 $\mu$M). To further confirm Cy5.5-A11 as a PD-L1-targeted probe for imaging of live cancer cells, we established stable PD-L1 knockdown MDA-MB-231, H460, and A375 cell lines (Figure 2B). PD-L1 knockdown and shNC control cell lines were incubated with 10 nM Cy5.5-A11 probe at 37 °C for 6 h and observed using laser confocal microscopy. As shown in Figure 2B, the fluorescent signal was seen in shNC control cells but not PD-L1 knockdown cancer cells, confirming the Cy5.5-A11 probe specifically targeting PD-L1. Taken together, the results demonstrate that Cy5.5-A11 serves as a PD-L1-targeted probe for *in vitro* imaging of multiple cancer cells.

***In Vivo* Fluorescence Imaging of Cy5.5-A11.** To ascertain the efficacy of Cy5.5-A11 for *in vivo* tumor imaging, subcutaneous xenografts of MDA-MB-231, H460, and A375 cells were established, and these mice received an intravenous injection of 1 nM Cy5.5-A11 and were subjected to whole-body imaging 0.5−24 h postinjection (p.i.) using the Caliper Lumina XR Imaging System. The results showed that Cy5.5-A11 exhibited rapid tumor imaging as quickly as 0.5 h p.i., with the tumor-specific fluorescence signal peaking at 2 h p.i. while remaining distinctly visible at 24 h p.i. (Figure 3A). High tumor-to-muscle fluorescence signal ratios of MDA-MB-231, H460, and A375 xenografts were noted at 0.5−6 h p.i. (Figure 3B). These results demonstrate that Cy5.5-A11 exhibits a robust capacity for *in vivo* tumor imaging.

To investigate the Cy5.5-A11 probe's tumor specificity, an *in vivo* blocking study of Cy5.5-A11 imaging was conducted. In the blocking group, tumor-bearing mice received intravenous injections of a mixture containing 1 nM Cy5.5-A11 and 1 $\mu$M unlabeled A11. In the nonblocking group, tumor-bearing mice received an intravenous injection of 1 nM Cy5.5-A11 only. Tumor-bearing mice in both groups were subjected to whole-body imaging at 4 h p.i. As shown in Figure 4A, excessive unlabeled A11 obviously blocked tumor uptake of Cy5.5-A11. Region-of-interest (ROI) analysis of each image was used to quantify tumor contrast. As shown in Figure 4B, the tumor-to-muscle tissue fluorescence ratios at 4 h p.i. were markedly decreased in the blocking group against the nonblocking group, which validates the Cy5.5-A11 probe's tumor specificity in whole-body imaging. To investigate the specificity of Cy5.5-A11 for PD-L1 imaging, PD-L1 knockdown tumor-bearing mice received an intravenous injection of 1 nM Cy5.5-A11 and were subjected to whole-body imaging at 4 h p.i. The result showed that the fluorescent signal of tumors and tumor-to-muscle tissue fluorescence ratios were dramatically decreased as compared to the nonblocking group (Figure 4A,B). Moreover, PD-L1 expression was not detected by IHC in the xenografts originating from PD-L1 knockdown cancer cells (Figure 4C). The results confirm the specificity of Cy5.5-A11 for PD-L1 imaging of tumors in the whole body.


https://doi.org/10.1021/acsomega.4c06761
*ACS Omega* 2024, 9, 43826−43833

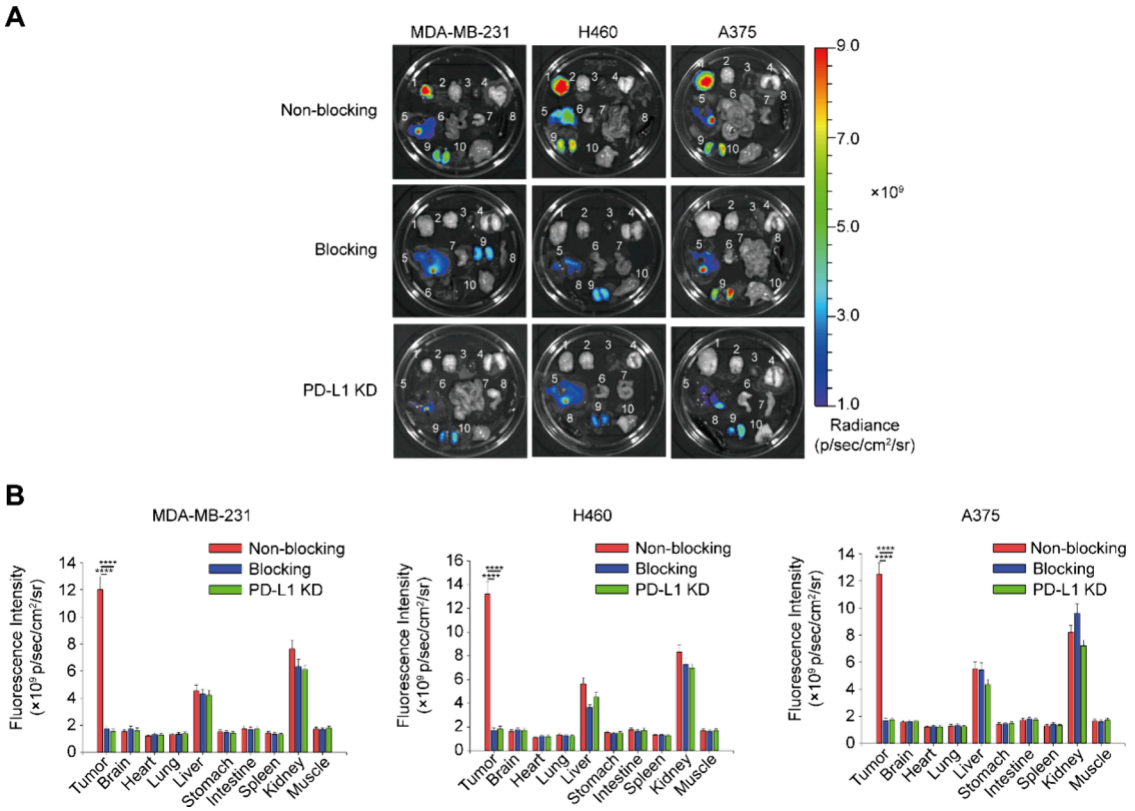


**Figure 5.** Biodistribution of Cy5.5-A11 in MDA-MB-231, H460, and A375 tumor-bearing mice at 4 h p.i. (A) Representative *ex vivo* fluorescent images of tumor and organs (1, tumor; 2, brain; 3, heart; 4, lung; 5, liver; 6, stomach; 7, intestine; 8, spleen; 9, kidney; 10, muscle) collected from the mice injected with 1.0 nM of Cy5.5-A11 with (blocking group) or without (nonblocking group and PD-L1 KD group) 1.0 $\mu$M unlabeled A11. (B) Fluorescence intensity of tumors and major organs according to ROI analysis at 4 h p.i.

***Ex Vivo* Biodistribution Study of Cy5.5-A11.** Tumors and major organs (brain, heart, lung, liver, stomach, intestine, spleen, lung, kidney, and muscle) from tumor-bearing mice were collected and *ex vivo* imaged, and quantification of optical *ex vivo* imaging was conducted in the ROI. As shown in Figure 5, the *ex vivo* results were consistent with the *in vivo* results. In the nonblocking group, significant uptake of the Cy5.5-A11 probe in the xenografts was observed at 4 h p.i., whereas excessive unlabeled A11 obviously reduced the uptake of Cy5.5-A11 in the xenografts (Figure 5A,B), supporting Cy5.5-A11's tumor specificity for *in vivo* imaging. Moreover, the fluorescent signal was dramatically decreased in the xenografts of cancer cells with PD-L1 knockdown (Figure 5A,B), supporting Cy5.5-A11's specificity for PD-L1 imaging of tumors. We also observed that the uptake of Cy5.5-A11 was higher in the liver and kidney than that in other organs in the three groups of mice (Figure 5A,B), indicating that Cy5.5-A11 probes were excluded mainly from the biliary and urinary system.

## DISCUSSION

PD-L1 is an important biomarker for selecting ICI therapy patients.[7] IHC of PD-L1 in tumor tissues obtained from invasive procedures is clinically used to assess the PD-L1 expression levels. Nonetheless, the PD-L1 expression levels may be truly reflected by an IHC-based assay due to tumor heterogeneity[14−17] and dynamic PD-L1 expression.[10,11] Consequently, it is important to develop molecular imaging techniques capable of noninvasively monitoring the dynamic expressions of PD-L1 *in vivo*.[27]

Based on the advantages of A11 peptide binding and degrading PD-L1, we developed an NIR optical imaging probe, Cy5.5-A11, for PD-L1 imaging of tumors. The *in vitro* imaging studies reveal Cy5.5-A11 as a PD-L1-targeted probe for *in vitro* imaging of triple-negative breast cancer, NSCLC, and melanoma cells. The *in vitro* imaging studies showed that Cy5.5-A11 promptly accumulated in the xenografts of triple-negative breast cancer, NSCLC, and melanoma cells as quickly as 0.5 h p.i. Subsequently, as nonspecific background signals decreased, tumor-specific fluorescent signals exhibited a high signal-to-noise ratio at 0.5−6 h p.i. and remained distinctly visible at 24 h p.i. These results indicate that Cy5.5-A11 possesses a strong ability for *in vivo* tumor imaging. We also observed that unlabeled A11 obviously blocked tumor uptake of Cy5.5-A11, resulting in notably lower tumor-to-muscle tissue fluorescence signal ratios at 4 h p.i. in the blocking group relative to the nonblocking group, while the fluorescence signal of other major organs was at a similar level in both blocking and nonblocking groups, which indicates the tumor specificity of the Cy5.5-A11 probe in whole-body imaging. Moreover, the fluorescent signal of tumors and tumor-to-muscle tissue fluorescence signal ratios were dramatically decreased in PD-L1 knockdown tumor-bearing mice, demonstrating the specificity of Cy5.5-A11 for PD-L1 imaging of tumors. The uptake of the Cy5.5-A11 probe in the liver and kidney exceeded that in other major organs, indicating that the biliary and urinary system is the probable route for Cy5.5-A11 probe excretion. The *ex vivo* imaging study showed significant uptake of the Cy5.5-A11 probe in the xenografts, liver, and kidney at 4 h p.i., indicating that Cy5.5-A11 was quickly cleared from


https://doi.org/10.1021/acsomega.4c06761
ACS Omega 2024, 9, 43826−43833

normal tissues. To our knowledge, it is for the first time reported that an NIR-labeled peptide probe is used for molecular imaging of PD-L1 in multiple cancers.

Recent years have witnessed that the NIR-labeled anti-PD-L1 antibody probe was utilized for molecular imaging of PD-L1 in mice carrying xenografts.[18,19] Several studies have also used PD-L1-targeting peptides labeled with radionuclides for noninvasive tumor imaging of PD-L1 in animals and humans.[28−31] These PD-L1 imaging probes can accurately detect PD-L1 expression in tumors and monitor immunotherapeutic response.[18,19,28−31] In this study, we developed an NIR-labeled peptide (Cy5.5-A11) for molecular imaging of PD-L1 in the xenografts. Peptides possess several advantages compared to PD-L1 antibodies, such as the absence of immune-related adverse events (irAEs), enhanced penetration into tumors, reduced immunogenicity, and simplicity of manufacturing.[32,33] Consequently, Cy5.5-A11 might be an optimal probe for *in vivo* tumor imaging of PD-L1 superior to NIR-PD-L1 antibody probes at least in tissue penetration, imaging speed, biocompatibility, and safety. Moreover, compared to the radiolabeled PD-L1-targeting peptides for noninvasive imaging of PD-L1, the NIR-labeled Cy5.5-A11 probe is nonradioactive, easy to synthesize, and possesses a high signal-to-noise ratio and tumor imaging ability, and the imaging instrument is portable.

In summary, our *in vivo* and *ex vivo* imaging investigations indicate that Cy5.5-A11 functions as a promising and reliable probe for visualizing PD-L1 levels in multiple cancers. The new peptide probe Cy5.5-A11, characterized by its high efficiency, sensitivity, and low immunogenicity, presents a promising NIR probe for the real-time, dynamic, and quantitative assessment of PD-L1 levels across multiple cancers, with potential implications for predicting responses to ICI therapy in cancer patients.

## EXPERIMENTAL SECTION

**Reagents.** PD-L1 rabbit mAb (#13684, CST), GAPDH mouse mAb (#AC002, ABclonal), HRP-conjugated anti-rabbit IgG (#7074, CST), HRP-conjugated anti-mouse IgG (#7076, CST), Lipofectamine 2000 (#11668019, Thermo Fisher Scientific). The lentiviral vector PLKO.1-shPD-L1 expressing PD-L1 shRNA was constructed by us. The designated sequence of shRNA targeting PD-L1 mRNA is 5′-CTGA-CATTCATCTTCCGTTTA-3′.[34]

**Cy5.5 Labeled ANXA1-Dereived Peptide A11.** ANXA1-derived 11-mer peptide (20−30aa) (EYVQTVKSSKG), A11, and Cy5.5-A11 peptides were synthesized by ChinaPeptides (Suzhou, China). The crude products underwent purification through high-performance liquid chromatography (HPLC), and their structures were confirmed via mass spectrometry (MS).

**Cell Lines and Culture.** MDA-MB-231, H460, and A375 cancer cell lines were purchased from the American Type Culture Collection (ATCC). Cells were maintained in Dulbecco's modified eagle medium (DMEM) or Roswell Park Memorial Institute (RPMI)-1640 medium supplemented with 10% fetal bovine serum (FBS, #A5256701,Thermo Fisher Scientific) at 37 °C in a 5% $CO_2$ atmosphere. All cell lines were authenticated through short tandem repeat (STR) profiling and were regularly screened for mycoplasma contamination.

**Stable Knockdown PD-L1 in Cancer Cell Lines.** Lentiviral vectors containing PD-L1 shRNA or scrambled shRNA (shNC) were employed to infect MDA-MB-231, H460, and A375 cell lines. The cells were subsequently selected using 1 mg/mL of puromycin (#A1113803, Thermo Fisher Scientific) for 2 weeks. Stable PD-L1 knockdown and shNC control cancer cell lines were generated, which was validated by Western blot analysis.

**Western Blot Analysis.** Proteins were extracted from indicated cells using RIPA lysis buffer containing protease inhibitors (#4693132001, Roche). The BCA protein assay reagent (#P0012, Beyotime) was employed to assess the protein concentration. For SDS-PAGE, 50 $\mu$g of protein from each sample was loaded and separated, followed by transfer to a poly (vinylidene difluoride) membrane (#ISEQ00010, Millipore). After blocking for 1 h at room temperature with blocking buffer (#P0023B, Beyotime), the membranes were incubated overnight at 4 °C with either anti-PD-L1 (1:1000 dilution) or anti-GAPDH antibody (1:2000 dilution). Subsequently, the membranes were incubated with HRP-conjugated anti-rabbit IgG (1:3000 dilution) or HRP-conjugated anti-mouse IgG (1:3000 dilution) for 2 h at room temperature. After washing, protein signals were visualized by using an enhanced chemiluminescence detection reagent (Roche).

***In Vitro* Fluorescence Imaging of Cy5.5-A11.** First, 5 $\times 10^4$ MDA-MB-231, H460, and A375 cancer cells were plated in chamber slides (#PEZGS0816, Millicell EZ), respectively, and cultured for 24 h. Afterward, cells were incubated with 10 nM Cy5.5-labeled A11 peptide (Cy5.5-A11) for 6 h. Cancer cells were incubated with a combination of 10 nM Cy5.5-A11 and 1 $\mu$M unlabeled A11 for 6 h in the blocking group. Following three washes with PBS, cells were fixed in 4% paraformaldehyde for 20 min and subsequently labeled with DAPI for viewing the nuclei. Images were acquired by using a confocal microscope.

***In Vivo* NIF Imaging and Biodistribution Study of Cy5.5-A11.** Five-week-old female BALB/c nu/nu nude mice were purchased from the Laboratory Animal Center of Central South University and kept in pathogen-free environments. All animal procedures adhered to the Guide for the Care and Use of Laboratory Animals at Xiangya Hospital, Central South University, and were approved by the Institutional Animal Ethics Committee. The subcutaneous xenografts were established by injecting 5 × $10^6$ cancer cells into the right shoulder of nude mice, respectively.

Upon reaching a tumor volume of 100 $mm^3$, the nonblocking group ($n$ = 3) received 1 nM Cy5.5-A11 peptide intravenously and followed up with optical imaging at predefined intervals. For the blocking group ($n$ = 3), a mixture of 1 nM Cy5.5-A11 peptide and 1 $\mu$M unlabeled A11 peptide was injected intravenously. The Caliper Lumina XR Imaging System with near-infrared fluorescent filter sets (PerkinElmer Inc., USA) was used for *in vivo* fluorescence imaging, and the corresponding IVIS Living Imaging 4.3.1 software was used for analysis. To measure the fluorescence intensity of Cy5.5-A11, a specific Cy5.5 filter set was utilized. Imaging was carried out under consistent illumination parameters, including lamp power, filters, f/stop, field of view, and binning. Fluorescence emission data were normalized and presented in terms of photons per second per centimeter squared per steradian (p/s/$cm^2$/sr). For all NIF images, an exposure period of 1 s (f/stop = 4) was used. Mice were sacrificed 4 h p.i., followed by excision of tumors and organs for *ex vivo* fluorescence imaging, with average fluorescence levels recorded for every specimen.


https://doi.org/10.1021/acsomega.4c06761
ACS Omega 2024, 9, 43826−43833

**Immunohistochemistry.** Immunohistochemical staining for PD-L1 was conducted on formalin-fixed and paraffin-embedded tissue sections. Briefly, tissue sections were deparaffinized, rehydrated, and subjected to antigen retrieval in a 10 mmol/L sodium citrate buffer (pH 6.0). After that, the tissue sections were treated in 3% hydrogen peroxide for 10 min to suppress endogenous peroxidase activity, preincubated with 10% nonimmune goat serum at room temperature for 15 min to block nonspecific binding of the antibody, and then incubated overnight at 4 °C with the anti-PD-L1 antibody (1:100 dilution; #213524, Abcam). Subsequently, the tissue sections were incubated with a biotinylated secondary antibody for 30 min at room temperature, followed by the incubation of the avidin−biotin peroxidase complex. Staining was performed with 3,3-diaminobenzidine (DAB, #D12384, Sigma-Aldrich). Finally, the tissue sections were counterstained with hematoxylin.

**Statistical Analysis.** The analysis of statistical data was conducted by utilizing IBM SPSS, while data visualization was accomplished by using GraphPad Prism. The ROI tool in IVIS Living Image 4.3.1 software was employed to evaluate tumor contrast by computing the mean fluorescence intensities of normal adjacent tissues and tumor tissues. Results are expressed as the mean ± the standard deviation. Comparisons between the two groups were conducted using Student's $t$ test, with $P$ values less than 0.05 deemed statistically significant.

## AUTHOR INFORMATION


### Corresponding Author

**Zhi-Qiang Xiao** − *Department of Pathology, Xiangya Hospital, Research Center of Carcinogenesis and Targeted Therapy, Xiangya Hospital, and The Higher Educational Key Laboratory for Cancer Proteomics and Translational Medicine of Hunan Province, Xiangya Hospital, Central South University, Changsha 410008, China; National Clinical Research Center of Geriatric Disorders, Xiangya Hospital, Central South University, Changsha 410011, China;* orcid.org/0000-0002-5127-586X; Phone: 86-731-89753378; Email: zhiqiangxiao@csu.edu.cn; Fax: 86-731-84327332

### Authors

**Xiao-Cheng Cao** − *Department of Pathology, Xiangya Hospital, Research Center of Carcinogenesis and Targeted Therapy, Xiangya Hospital, and The Higher Educational Key Laboratory for Cancer Proteomics and Translational Medicine of Hunan Province, Xiangya Hospital, Central South University, Changsha 410008, China; National Clinical Research Center of Geriatric Disorders, Xiangya Hospital, Central South University, Changsha 410011, China*

**Xue-Li Mao** − *Research Center of Carcinogenesis and Targeted Therapy, Xiangya Hospital and The Higher Educational Key Laboratory for Cancer Proteomics and Translational Medicine of Hunan Province, Xiangya Hospital, Central South University, Changsha 410008, China*

**Shan-Shan Lu** − *Research Center of Carcinogenesis and Targeted Therapy, Xiangya Hospital and The Higher Educational Key Laboratory for Cancer Proteomics and Translational Medicine of Hunan Province, Xiangya Hospital, Central South University, Changsha 410008, China*

**Wei Zhu** − *Department of Pathology, Xiangya Hospital, Central South University, Changsha 410008, China; National Clinical Research Center of Geriatric Disorders, Xiangya Hospital, Central South University, Changsha 410011, China*

**Wei Huang** − *Research Center of Carcinogenesis and Targeted Therapy, Xiangya Hospital and The Higher Educational Key Laboratory for Cancer Proteomics and Translational Medicine of Hunan Province, Xiangya Hospital, Central South University, Changsha 410008, China*

**Hong Yi** − *Research Center of Carcinogenesis and Targeted Therapy, Xiangya Hospital and The Higher Educational Key Laboratory for Cancer Proteomics and Translational Medicine of Hunan Province, Xiangya Hospital, Central South University, Changsha 410008, China*

**Li Yuan** − *Department of Nuclear Medicine, The Third Xiangya Hospital, Central South University, Changsha 410013, China*

**Jian-Hua Zhou** − *Department of Pathology, Xiangya Hospital, Central South University, Changsha 410008, China; National Clinical Research Center of Geriatric Disorders, Xiangya Hospital, Central South University, Changsha 410011, China*

Complete contact information is available at: https://pubs.acs.org/10.1021/acsomega.4c06761

### Author Contributions

#X.-C.C. and X.-L.M. contributed equally.


### Notes

The authors declare no competing financial interest.

## ACKNOWLEDGMENTS

This study was supported by the National Natural Science Foundation of China (82073005 to Z.-Q.X., 82103638 to S.-S.L., and 82172678 to L.Y.) and the Key Research and Development Program of Hunan Province of China (2022SK2058 to Z.-Q.X.).

## REFERENCES

(1) Brahmer, J. R.; Tykodi, S. S.; Chow, L. Q.; Hwu, W. J.; Topalian, S. L.; Hwu, P.; Drake, C. G.; Camacho, L. H.; Kauh, J.; Odunsi, K.; et al. Safety and activity of anti-PD-L1 antibody in patients with advanced cancer. *N. Engl. J. Med.* **2012**, *366*, 2455−2465.

(2) Zou, W.; Wolchok, J. D.; Chen, L. PD-L1 (B7-H1) and PD-1 pathway blockade for cancer therapy: Mechanisms, response biomarkers, and combinations. *Sci. Transl. Med.* **2016**, *8*, 328rv4.

(3) Jiang, X.; Wang, J.; Deng, X.; Xiong, F.; Ge, J.; Xiang, B.; Wu, X. J.; Zhou, M.; Li, X.; Li, Y.; et al. Role of the tumor microenvironment in PD-L1/PD-1-mediated tumor immune escape. *Mol. Cancer* **2019**, *18*, 10.

(4) Schildberg, F. A.; Klein, S. R.; Freeman, G. J.; Sharpe, A. H. Coinhibitory Pathways in the B7-CD28 Ligand-Receptor Family. *Immunity.* **2016**, *44*, 955−972.

(5) Dong, H.; Strome, S. E.; Salomao, D. R.; Tamura, H.; Hirano, F.; Flies, D. B.; Roche, P. C.; Lu, J.; Zhu, G.; Tamada, K.; et al. Tumor-associated B7-H1 promotes T-cell apoptosis: a potential mechanism of immune evasion. *Nat. Med.* **2002**, *8*, 793−800.

(6) Ren, D.; Hua, Y.; Yu, B.; Ye, X.; He, Z.; Li, C.; Wang, J.; Mo, Y.; Wei, X.; Chen, Y.; et al. Predictive biomarkers and mechanisms underlying resistance to PD1/PD-L1 blockade cancer immunotherapy. *Mol. Cancer.* **2020**, *19*, 19.

(7) Yi, M.; Jiao, D.; Xu, H.; Liu, Q.; Zhao, W.; Han, X.; Wu, K. Biomarkers for predicting efficacy of PD-1/PD-L1 inhibitors. *Mol. Cancer.* **2018**, *17*, 129.

(8) Patel, S. P.; Kurzrock, R. PD-L1 Expression as a predictive biomarker in cancer Immunotherapy. *Mol. Cancer Ther.* **2015**, *14*, 847−856.
(9) Brody, R.; Zhang, Y.; Ballas, M.; Siddiqui, M. K.; Gupta, P.; Barker, C.; Midha, A.; Walker, J. PD-L1 expression in advanced NSCLC: Insights into risk stratification and treatment selection from a systematic literature review. *Lung Cancer.* **2017**, *112*, 200−215.
(10) Ibrahim, D.; Simó, C.; Brown, E. L.; Shmuel, S.; Panikar, S. S.; Benton, A.; DeWeerd, R.; Dehdashti, F.; Park, H.; Pereira, P. M. R. PD-L1 has a heterogeneous and dynamic expression in gastric cancer with implications for immunoPET. *Front. Immunol.* **2024**, *15*, No. 1405485.
(11) Choe, E. A.; Cha, Y. J.; Kim, J. H.; Pyo, K. H.; Hong, M. H.; Park, S. Y.; Shim, H. S.; Jung, I.; Lee, C. Y.; Cho, B. C.; Kim, H. R. Dynamic changes in PD-L1 expression and CD8(+) T cell infiltration in non-small cell lung cancer following chemoradiation therapy. *Lung Cancer.* **2019**, *136*, 30−36.
(12) Shen, X.; Zhang, L.; Li, J.; Li, Y.; Wang, Y.; Xu, Z. X. Recent Findings in the Regulation of Programmed Death Ligand 1 Expression. *Front. Immunol.* **2019**, *10*, 1337.
(13) Kordbacheh, T.; Honeychurch, J.; Blackhall, F.; Faivre-Finn, C.; Illidge, T. Radiotherapy and anti-PD-1/PD-L1 combinations in lung cancer: building better translational research platforms. *Ann. Oncol.* **2018**, *29*, 301−310.
(14) Ilie, M.; Hofman, V.; Dietel, M.; Soria, J. C.; Hofman, P. Assessment of the PD-L1status by immunohistochemistry: challenges and perspectives for therapeutic strategies in lung cancer patients. *Virchows. Arch.* **2016**, *468*, 511−525.
(15) Wang, Y.; Zhou, Y.; Yang, L.; Lei, L.; He, B.; Cao, J.; Gao, H. Challenges Coexist with Opportunities: Spatial Heterogeneity Expression of PD-L1 in Cancer Therapy. *Adv. Sci.* **2024**, *11*, No. e2303175.
(16) Kunimasa, K.; Hirotsu, Y.; Amemiya, K.; Honma, K.; Nakamura, H.; Nishino, K.; Omata, M. Genetic dissection of intratumor heterogeneity of PD-L1 expression in EGFR-mutated lung adenocarcinoma. *Thorac. Cancer.* **2023**, *14*, 2210−2215.
(17) Broos, K.; Lecocq, Q.; Raes, G.; Devoogdt, N.; Keyaerts, M.; Breckpot, K. Noninvasive imaging of the PD-1: PD-L1 immune checkpoint: Embracing nuclear medicine for the benefit of personalized immunotherapy. *Theranostics.* **2018**, *8*, 3559−3570.
(18) Liu, Q.; Tian, J.; Tian, Y.; Sun, Q.; Sun, D.; Wang, F.; Xu, H.; Ying, G.; Wang, J.; Yetisen, A. K.; et al. Near-Infrared-II Nanoparticles for Cancer Imaging of Immune Checkpoint Programmed Death-Ligand 1 and Photodynamic/Immune Therapy. *ACS. Nano.* **2021**, *15*, 515−525.
(19) Zhang, M.; Jiang, H.; Zhang, R.; Jiang, H.; Xu, H.; Pan, W.; Gao, X.; Sun, Z. Near-infrared fluorescence-labeled anti-PD-L1-mAb for tumor imaging in human colorectal cancer xenografted mice. *J. Cell. Biochem.* **2019**, *120*, 10239−10247.
(20) Chatterjee, S.; Lesniak, W. G.; Nimmagadda, S. Noninvasive imaging of immune checkpoint ligand PD-L1 in tumors and metastases for guiding immunotherapy. *Mol. Imaging* **2017**, *16*, No. 1536012117718459.
(21) Yu, Z. Z.; Liu, Y. Y.; Zhu, W.; Xiao, D.; Huang, W.; Lu, S. S.; Yi, H.; Zeng, T.; Feng, X. P.; Yuan, L.; et al. ANXA1-derived peptide for targeting PD-L1 degradation inhibits tumor immune evasion in multiple cancers. *J. Immunother. Cancer.* **2023**, *11*, No. e006345.
(22) Luker, G. D.; Luker, K. E. Optical imaging: current applications and future directions. *J. Nucl. Med.* **2008**, *49*, 1−4.
(23) Liu, Z.; Li, Z. Molecular imaging in tracking tumor-specific cytotoxic T lymphocytes (CTLs). *Theranostics.* **2014**, *4*, 990−1001.
(24) Kosaka, N.; Ogawa, M.; Choyke, P. L.; Kobayashi, H. Clinical implications of near-infrared fluorescence imaging in cancer. *Future Oncol.* **2009**, *5*, 1501−1511.
(25) Luo, S.; Zhang, E.; Su, Y.; Cheng, T.; Shi, C. A review of NIR dyes in cancer targeting and imaging. *Biomaterials.* **2011**, *32*, 7127−7138.
(26) Rudin, M.; Weissleder, R. Molecular imaging in drug discovery and development. *Nat. Rev. Drug. Discovery* **2003**, *2*, 123−131.
(27) Ehlerding, E. B.; England, C. G.; McNeel, D. G.; Cai, W. Molecular Imaging of Immunotherapy Targets in Cancer. *J. Nucl. Med.* **2016**, *57*, 1487−1492.
(28) De Silva, R. A.; Kumar, D.; Lisok, A.; Chatterjee, S.; Wharram, B.; Venkateswara Rao, K.; Mease, R.; Dannals, R. F.; Pomper, M. G.; Nimmagadda, S. Peptide-Based $^{68}$Ga-PET Radiotracer for Imaging PD-L1 Expression in Cancer. *Mol. Pharmaceutics* **2018**, *15*, 3946−3952.
(29) Zhou, X.; Jiang, J.; Yang, X.; Liu, T.; Ding, J.; Nimmagadda, S.; Pomper, M. G.; Zhu, H.; Zhao, J.; Yang, Z.; Li, N. First-in-Humans Evaluation of a PD-L1-Binding Peptide PET Radiotracer in Non-Small Cell Lung Cancer Patients. *J. Nucl. Med.* **2022**, *63*, 536−542.
(30) Mishra, A.; Gupta, K.; Kumar, D.; Lofland, G.; Sharma, A. K.; Solnes, L. B.; Rowe, S. P.; Forde, P. M.; Pomper, M. G.; Gabrielson, E. W.; Nimmagadda, S. Non-invasive PD-L1 quantification using [$^{18}$F]DK222-PET imaging in cancer immunotherapy. *J. Immunother. Cancer.* **2023**, *11*, No. e007535.
(31) Zhu, S.; Liang, B.; Zhou, Y.; Chen, Y.; Fu, J.; Qiu, L.; Lin, J. Development of novel peptide-based radiotracers for detecting PD-L1 expression and guiding cancer immunotherapy. *Eur. J. Nucl. Med. Mol. Imaging.* **2024**, *51*, 625−640.
(32) Erak, M.; Bellmann-Sickert, K.; Els-Heindl, S.; Beck-Sickinger, A. G. Peptide chemistry toolbox - Transforming natural peptides into peptide therapeutics. *Bioorg. Med. Chem.* **2018**, *26*, 2759−2765.
(33) Shaabani, S.; Huizinga, H. P. S.; Butera, R.; Kouchi, A.; Guzik, K.; Magiera-Mularz, K.; Holak, T. A.; Dömling, A. A patent review on PD-1/PD-L1 antagonists: small molecules, peptides, and macrocycles (2015−2018). *Expert. Opin. Ther. Pat.* **2018**, *28*, 665−678.
(34) Liu, Y.; Li, X.; Zhang, H.; Zhang, M.; Wei, Y. HuR up-regulates cell surface PD-L1 via stabilizing CMTM6 transcript in cancer. *Oncogene.* **2021**, *40*, 2230−2242.


https://doi.org/10.1021/acsomega.4c06761
*ACS Omega* 2024, 9, 43826−43833